ACTUATION SYSTEMS FOR RAISED KRUEGER FLAPS ON LAMINAR AIRFOILS

K. Krall*, L. Böhme*, F. Thielecke*

* Hamburg University of Technology, Institute of Aircraft Systems Engineering,

Nesspriel 5, 21129 Hamburg, Germany

Abstract

Laminarization of airfoils offers great potential for improving aerodynamic performance and presents a key aspect of research in the optimization of modern commercial aircraft. Still, a challenge to be faced is potential contamination of the wing's leading edge, which creates turbulence wedges that prevent maintained laminar flow. The raised bull-nose Krueger flap poses a solution to this by shielding the leading edge and thus protecting the wing from contamination. However, an actuation system fulfilling the requirements resulting from this concept is yet to be developed and proven. The aim of this paper is to present a feasible actuation system concept for these control devices, while indicating challenges and limitations.

Keywords

Laminar wing, Krueger flap, actuation system, high lift, systems architecture, system design

1. INTRODUCTION

The aerodynamic advantages of reducing friction drag of the wing profile by means of natural laminar flow have been discussed by various publications. Especially the innovative wing design method of the Crossflow Attenuated Natural Laminar Flow (CATNLF) promises significant extent of laminar flow at the cruise condition, resulting in a potential fuel burn reduction of up to 10% depending on the configuration However, the [1][2][3]. contamination of the leading edge of the wing caused by insects or dust particles in low altitudes creates turbulence wedges that prevents maintained laminar flow. A solution to this problem presents the raised bull-nose Krueger flap. This concept is characterized by the flap being positioned in a recess at the bottom side of the wing during cruise and is deployed in front of the leading edge in lower altitudes for protection purposes. Positioning the flap in a recess at the wing's bottom side ensures undisturbed airflow over the low pressure side of the airfoil, due to the lack of system and irregularities. components The aerodynamic performance of such a high lift configuration was recently investigated by the EU-project UHURA [4], but the system technical feasibility remains to be investigated.

Architecture Design poses a complex challenge. For once, high actuation loads must be generated due to the fact that the flaps motion opposing the aerodynamic loads main direction. Secondly, significant actuation speeds arise, due to the notable traversing distance between retracted and deployed positions. Furthermore, intricate safety prerequisites have to considered. The development of thinner wing profiles creates an additional difficulty to implement high-performance actuation systems in the resulting confined installation space. An iterative system design and modelling process is required to investigate the technical feasibility for this raised Krueger high lift system. The aim of this study is to detect limits and define recommended measures regarding the system design for the use of this novel application of Krueger flaps.

For this purpose, the requirements and conditions are defined in section 2. The design process of the system architecture of the high lift system as well as the result is presented in section 3. Based on the previous sections, simulation models are introduced and the installation space, safety aspects and mass will be discussed in section 4, yielding a first evaluation of feasibility of the system. The simulation model for final performance analysis as well as the obtained results are introduced in section 5.

2. REQUIREMENTS AND CONDITIONS

The aircraft configuration discussed in this paper, which represents a short- to medium-range aircraft with a high aspect ratio laminar wing is depicted in figure 1.

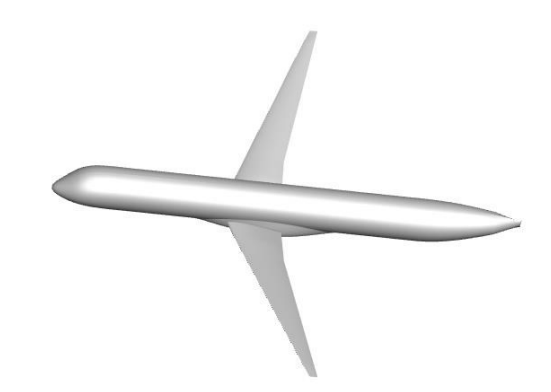


FIGURE 1. Three-dimensional representation of the aircraft configuration

To shield the wing from potential contamination and thus enable laminarity seven raised bull-nose Krueger flaps are positioned on the leading edge of the wing. These high lift devices fold out from the wing's lower surface in a rotary motion and position themselves in front of the leading edge in their final position. Thus, the wing is protected from contamination while a higher lift coefficient can be provided.

Contrary to other high lift devices, Krueger flaps enable a seamless surface on the wing's upper side, thus allowing laminar flow downstream of the front spar [5]. The folding rounded bull-nose additionally allows attached flow over a larger angle-of-attack [5]. Depending on the configuration and level of optimization, similar aerodynamic performance for Krueger flaps compared to slats can be achieved [5]. The movement of the Krueger flaps is shown in figure 2. As depicted, the bull-nose is an independent body rotating around the flap panel to reduce drag during the transition process, especially in the indicated critical transition range, and minimize the installation space requirements.

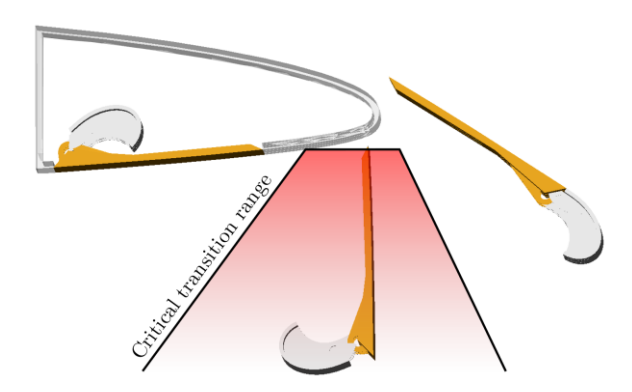


FIGURE 2. Schematic representation of the raised bullnose Krueger flap movement

As indicated in figure 2, a critical transition range between 50° and 110° deflection angle exists. If a Krueger flap is stuck in this range due to jamming in the system or in the kinematics, maximum air resistance is generated and the effectiveness of the trailing edge devices is significantly impaired. In particular, a deterioration of the aileron effectiveness could then lead to hazardous reduction of control authority. The segmentation of wing movables of the reference aircraft is given in figure 3.



FIGURE 3. Control device segmentation projected on a schematic rectangular wing

A total of seven Krueger flaps are positioned at the leading edge, while the control surfaces located at the trailing edge consist of an inner flap, four MFCDS and four ailerons. According to the device segmentation given in figure 3, it is evident that the outer three Krueger flaps must never jam simultaneously in the critical transition range to ensure sufficient roll authority can be provided by the ailerons. Despite the fact that Krueger flap 5 is not positioned directly in front of the ailerons, crossflows arising from the wing's sweep would impair the ailerons effectivity. This requires sequential actuation of the outer Krueger flaps.

Due to a comparatively larger area of the two innermost Krueger flaps a higher torque demand is anticipated in order to move the flaps. To reduce the resulting load on the corresponding drive unit and increase partial availability, An individual actuation of the inner devices is considered reasonable.

In contrast, a simultaneous actuation of Krueger flaps 3 and

4 in a moderate load increase on the drive units and no critical impairment of the trailing edge devices. Thus, driving these leading edge devices simultaneously would result in a beneficial reduction of transition time.

The maximum transition time is set to be 40 seconds per the system requirements, assuming the degradation of the drive system. Additionally, the failure probability of one Krueger flap system shall be within a range of 10⁻⁵ and the total power shall not exceed 5 kW. Further CS-25 requirements, like symmetry of both wing sides, have to be considered as well [6].

3. DRIVE SYSTEM ARCHITECTURE

Based on the requirements detailed in section 2, potential kinematics were investigated. In particular, two concepts were identified as candidate solutions.

The goose-neck or swan-neck kinematic installed exemplary in the *Boeing 737*, *Boeing 757* and inboard rigid devices of the *Boeing 747*, which was further researched and developed in the EU-projects AFLoNext [7] and UHURA [8]. "The kinematic concept designed during the UHURA project is illustrated in figure 4. The goose-neck, which acts as a hinge and thus guides the rotational movement of the Krueger flap, is positioned close to the leading edge. The pivot point of the driving lever and thus connection to the drive system is positioned closer to the front spar to maximize potential installation space. To prevent collision of the goose-neck with the wing structure a cut out at the lower wing geometry is needed. The form fit between the goose-neck and drive lever in the extended position reduces the load on the drive system.

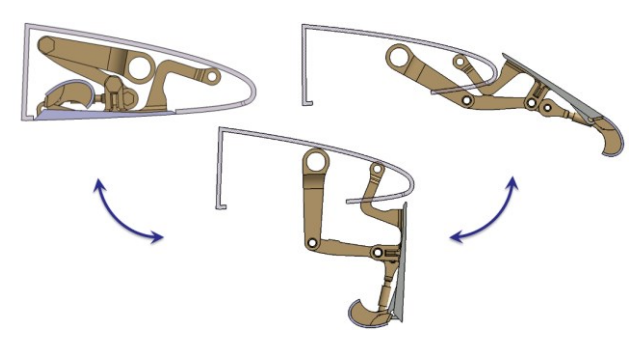


FIGURE 4. Optimized goose-neck kinematic [8]

An alternative concept is found in the four-bar linkage, which is applied on the outboard variable camber Krueger flaps of the *Boeing 747*, but can also be applied to fixed-shape panels. As shown in figure 5, the kinematic is rotationally driven. The rotation of the flap panel and the bullnose is achieved by a scissor-like motion of the rods. This kinematic offers great flexibility in the trajectory design of the panel and bullnose. Conversely, the connection to the drive system is positioned closely to the leading edge resulting in a minimization of available installation space for the system components.

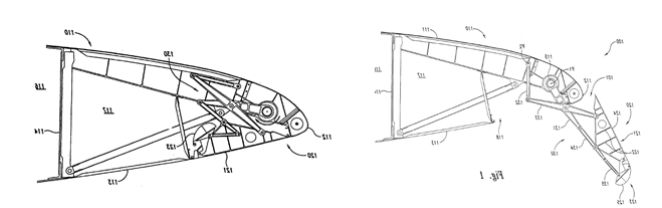


FIGURE 5. Four-bar linkage kinematic [9]

2

©2024

Due to lower complexity, larger available installation space, a preferable force flow and use in recent research projects, the goose-neck kinematic concept was deemed to be advantageous for the defined task and was chosen for further work.

As defined in section 2 the probability for multiple jammed Krueger flaps in the critical transition range must be reduced to a minimum. To meet this requirement, a sequential actuation of the Krueger flaps is used. This is depicted in figure 6 for a deployment starting at 2 seconds and ending at 20.7 seconds and subsequent retraction starting at 30 seconds and ending at 50 seconds. The process time difference between the deployment and retraction phase results from the critical transition range definition from 50° to 110°, as depicted in figure 2. Since the maximum deflection angle is determined to be 148°, the distance to the critical transition range at the start of the retraction process is 38°. At the start of deployment, the distance to the critical transition range amounts to 50°. Thus, more time is required for a Krueger flap to reach the critical transition range during deployment. Consequently, the following Krueger flap can be actuated earlier compared to the retraction process.

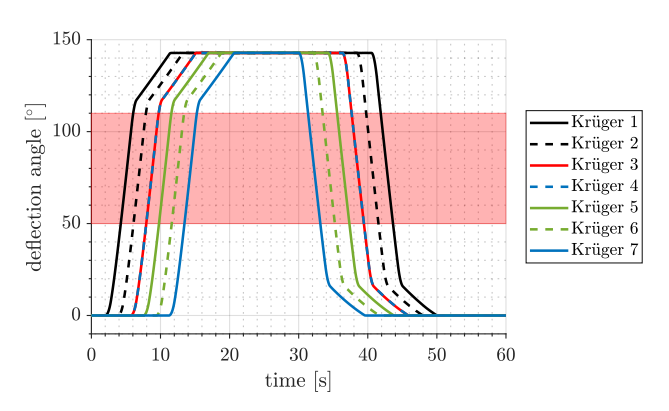


FIGURE 6. Sequential actuation of the Krueger flaps with indicated critical transition range (red)

The procedure starts with the deployment of the innermost Krueger flap. When this flap approaches the end of the critical transition range, the neighbouring device Is extended, leading to Krueger flap 2 entering into the critical transition range at the same time Krueger flap 1 is exiting it. This operation continues until the final position of the outermost flap is reached, concluding the deployment process. Therefore, a maximum of six Krueger drive systems are powered concurrently. As mentioned in section 2 Krueger flap 3 and 4 were chosen to be actuated simultaneously to reduce total transition time. The retraction procedure represents the reverse pattern starting with the outermost Krueger flap 7 and ending with the innermost Krueger flap 1.

Based on the defined requirements and selected kinematic the system architecture illustrated in figure 7 was developed. As shown in figure 7 each Krueger flap is actuated by a single drive system except for Krueger flaps 3 and 4, which share a grouped drive system. Both the single and the grouped drive systems are similar in the topology of the architecture, both consisting of a local power drive unit (PDU) connected to an offset gearbox (OG), which transfers the mechanical power of the PDU to the drive shaft.

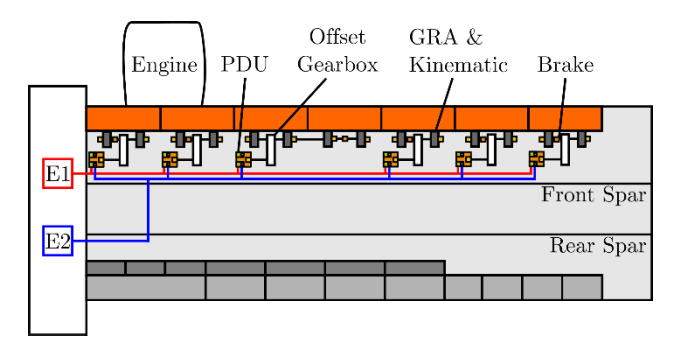


FIGURE 7. Schematic representation of the Krueger flap system architecture

Two redundant electrical supply systems provide power to the PDUs. The OG is needed to meet the installation space restrictions, which are especially challenging regarding the placement of the PDU. The drive shaft is positioned concentric to the geared rotary actuators (GRA), which are in turn connected to the goose-neck kinematic detailed above. Additionally, a brake is installed on the drive shaft. A more detailed depiction of a single drive system is given in figure 8.

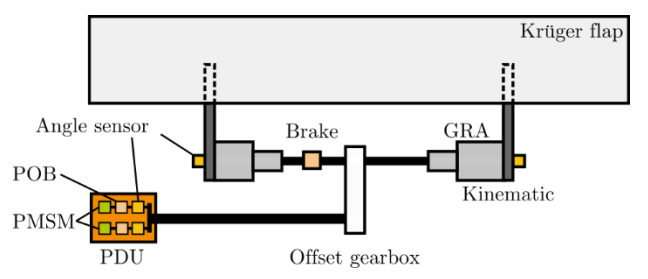


FIGURE 8. Schematic representation of a Krueger flap single drive system

As shown in figure 8, the PDU consists of two redundant pressure-off brakes (POB) and two redundant permanent magnet synchronous motors (PMSM), which are connected via a speed summing differential gearbox. Every PMSM is equipped with a dedicated motor control electronic (MCE), each supplied by an independent electrical supply system. This represents a conservative approach, similar to conventional high lift systems. This initial design is chosen to ensure a high availability for every Krueger flap. Future work shall optimize this drive unit composition to reduce system complexity. Minimizing the number of MCEs could greatly reduce maintenance efforts and should therefore be prioritized.

Angular position sensors are included at the output of the PMSMs for control and monitoring purposes. To detect potential fault scenarios, angular sensors are positioned at the GRA outputs, thus covering all relevant failures in the system (e. g. disconnect, jam or runaway) and all relevant failures in the structure (e. g. jam of the kinematic or freewheel of the GRA). The OG is positioned centred between the GRAs. Consequently, a drive through of the GRAs, which would result in higher complexity and size increase of the actuators, can be avoided.

The drive system used for Krueger flap 3 and 4 is equipped with two additional GRAs. The architecture for this grouped system resembles that of the single drive, apart from the drive shaft passing through the outer GRA of Krueger flap 3 and the inner GRA of Krueger flap 4 via a drive through shaft integrated in the actuators. The resulting size increase of the GRAs due to the drive through was assessed to be

in the limits of the installation space requirements. For the grouped drive, the brake is located between the actuators of Krueger flap 4.

As shown in figure 6, the transition time for deploying or retracting the Krueger flaps respectively amounts to around 20 seconds under nominal conditions. In the event of an electrical supply system failure, electrical power would only be supplied to half the PMSMs, consequently halving of all shaft drive speeds. Thus, the total transition time doubles to 40 seconds under this failure condition. Nevertheless, the requirements introduced in section 2 can still be met by this architecture design.

4. PRELIMINARY SIZING

For safety critical application, an investigation of reliability and safety of the system is indispensable. Furthermore, other criteria including mass and required installation space must be analyzed in order to evaluate the overall system architecture. A preliminary investigation of PMSMs, gears, actuators, brakes, shafts, sensors and cables has been conducted.

4.1. Safety Analysis

On the basis of the presented drive system architecture a safety analysis is carried out to assess whether the requirements set out in section 2 can be met. For this purpose, a Common Cause Analysis (CCA) based on the SAE guideline ARP 4761 [10] is conducted. Additionally, the failure rate of the total Krueger flap system architecture is determined.

To accommodate the requirements of the Common Mode Analysis (CMA), covering the potential failure of several components or systems as a result of a single cause, redundancy in signal and supply networks are necessary for the proposed system architecture. This is realized by utilizing two independent electrical supply systems and two redundant motor control electronics for each PDU. Hereby, loss of function following a common cause of failure is mitigated.

A particularly critical source for zonal damage, investigated during the Zonal Safety Analysis (ZSA), is represented by the rotor burst, defined by turbine blades detaching and damaging the structure [11]. This hazardous area affected by such a rotor burst lies between engine and fuselage. Based on the electrical supply routing and system architecture depicted in figure 7 only the inner Krueger flap is susceptible to failure due to a rotor burst.

To finalize the CCA, a Particular Risk Analysis (PRA) is conducted considering disturbances, that occur outside the system boundary and might lead to simultaneous failure of several subsystems, such as fire, non-containment of high energy devices (e. g. rotor burst), lightning strike or bird strike. It is assumed that all relevant scenarios are accounted for by conventionally used prevention methods, such as using low-flammable hydraulic fluids, structural protection from precipitation or external force and electrical shielding of the components.

To determine the failure rate of the chosen system architecture, Reliability Block Diagrams (RBD) are used. Exemplary the generated RBD for one single drive Krueger flap system is depicted in figure 9. The RBD representing the grouped drive system of Krueger flap 3 and 4 is almost identical, the only difference being two additional GRAs and angular sensors.

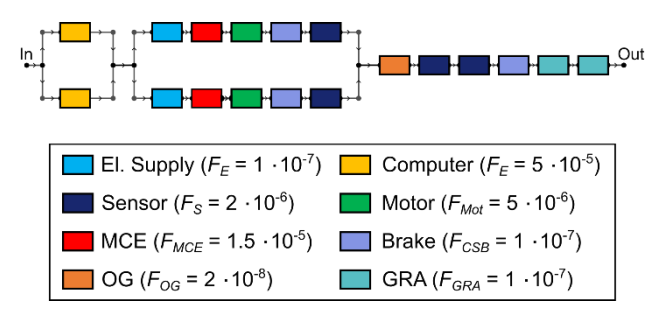


FIGURE 9. RBD of a single drive Krueger flap system

From the RBDs of the individual drive systems, the total reliability for both wings is determined to be $6.0\cdot 10^{-5}~1/f_h$. This represents the failure probability of one Krueger flap drive system on the total aircraft and will not lead to unsafe flight conditions. The deployment state of the respective device can be synchronized on the other wing side to avoid one-sided drag increase. Thus, the reliability requirement established in section 2 is fulfilled.

4.2. Mass and Installation Space

Following the proof of reliability, a preliminary sizing of system components has been conducted. In particular, mass, required installation space and power consumption were investigated. For this purpose, the gear ratios of the corresponding components and the resulting rotational speed of the drive shaft as well as PDU output must be defined. In cooperation with Liebherr Aerospace GmbH the GRAs were defined with a gear ratio of $i_{GRA} = 250$. Therefore, the loads on the remaining system components, especially the PMSMs, are reduced to a minimum. The rationale for incorporating OGs into the system architecture is to allow for a repositioning of the PDUs. Thus, their gear ratio is initially set to $i_{OG} = 1$. To further reduce the load on the drive units the PMSMs are equipped with an output stage gearbox, which enables an additional gear ratio of $i_{PMSM} = 4$. From these parameters, the required rotational velocity of the PMSMs for the sequential actuation defined in section 3 equates to $n_{Mot} = 5832 U/min$.

To determine the loads acting on the components aerodynamic forces acting on the Krueger flaps were determined by the Deutsches Zentrum für Luft- und Raumfahrt e.V. (DLR). Based on this data relevant design cases can be derived for the goose-neck kinematic specified in section 3. In this regard the maximum loads acting on the GRA outputs are detailed in figure 10 for the critical design case for a deployment and consequent retraction process as depicted in figure 6.

It must be noted that a change of load direction is present for all Krüger flaps as a result of their respective movement. In retracted position the aerodynamic loads act in deployment direction. During the deployment process, the load on the GRAs rises gradually due to the increase of drag caused by the flap panel rotation against the aerodynamic forces. The torque acting on the GRA decreases while the panel is still within the critical transition range due to lift increasing, thus lowering the required driving torque initially caused by aerodynamic drag. Eventually this results in an equilibrium, where no load is acting on the GRAs, at an approximate deflection of 111° to 126° depending on the Krueger flap and the direction of movement. The force resulting from the generated lift ultimately surpasses the the drag and negative torque appears at the GRAs. The retraction process reverses this

©2024

load progress by starting at the maximum deflection angle and thus the aerodynamic load opposes the direction of movement. It shall be noted that the aerodynamic forces differ between the deployment and retraction process.

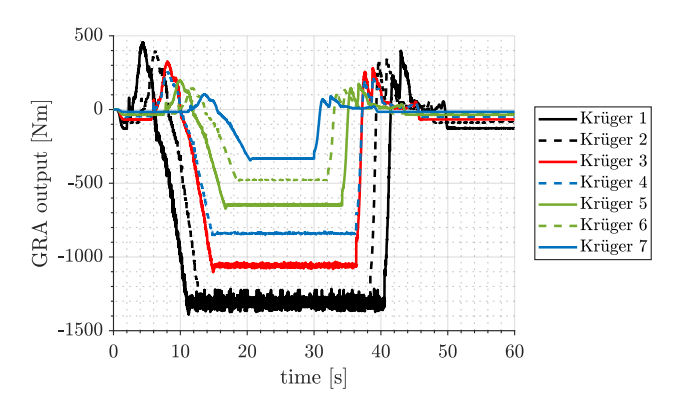


FIGURE 10. GRA output loads for critical design case

The GRA output loads during transition results in the following conclusion: In retracted position the flaps will be pulled out by the aerodynamic forces. Therefore, no driving power is needed to initiate the deployment process. After the initial movement of the flaps however, the driving torque increases to overcome the rising aerodynamic forces. After exceeding the deflection angle of aerodynamic equilibrium of the respective Krueger flap, the lift increases and thus actively pushes the panel to higher deflection angles. To prevent sudden inadvertent deflection of the flaps the PMSMs are required to change their direction of load to slow down the movement of the panels. This rapid change in motor torque demands highly adaptable and accurate control.

With the information on operating conditions, system component masses can be determined. In this regard, the shafts must be design to withstand critical failure conditions. In particular, the failure condition of jamming is seen as the dimensioning load case for this application. The cable mass estimation is divided into power supply and signal cables. To minimize weight +/- 270 VDC buses are chosen for the two electrical supplies providing power to the components, due to their potential beneficial distribution and equipment weight reduction [12][13]. To ensure availability, each motor, brake and sensor is connected with an individual signal cable The same reference point is thus used for both cable types. The weight of system components, such as motors, brakes and GRAs, are determined via knowledgebased methods. This results in the system mass estimation for both wing sides given in table 1. The given mass value for the shaft elements includes gear boxes and bearings. Compared to the drive system of conventionally used leading edge high-lift devices, such as slats, the proposed Krueger flap drive system results in a higher total mass. A conducted preliminary analysis of a slat high-lift system substituting the Krueger flaps system for the reference aircraft has resulted in a total system mass of 240 kg. The increased mass of the Krueger system was to be expected, since higher loads are acting on the Krueger panels and bull-noses and a higher actuation speed is required due to the greater range of motion of the Krueger system, compared to a slat mechanism.

However, additional benefits resulting from the use of Krueger flaps have to be taken into account. The shielding function combined with lesser flow disturbance on the upper wing surface by retracting the flap below the wing, enables the possibility of a maintained laminar flow, which in turn reduces drag, fuel consumption and thus mass of the total aircraft.

PDUs	76 kg
GRAs	139 kg
Shaft elements	60 kg
Brakes	18 kg
Sensors	27 kg
Cables	70 kg
Total	390 kg

TAB 1. Mass estimation breakdown of system components

The outcome of preliminary component sizing in regard to available installation space is depicted in figure 11. This analysis revealed sufficient installation space for the inner Krueger flaps 1-5, but a front spar conflict for the outer Krueger flaps 6 and 7. Challenging installation space requirements at the outer wing sections were to be expected due to the tapering of the wing (not shown in the simplified depiction in figure 11) resulting in reduced profile dimensions and thus reduced installation space. The PDUs represent the largest system elements. To accommodate the system components inside this restrictive space without changing the geometry of the Krueger flaps, the PDUs, have to be repositioned further towards the trailing edge, which results in the aforementioned front spar penetration.

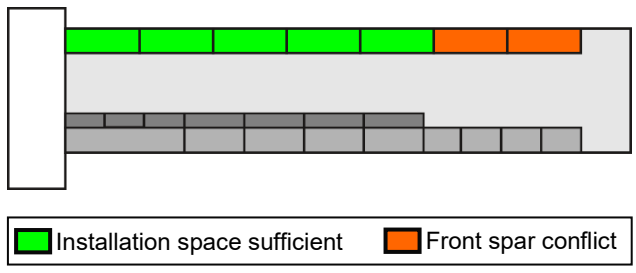


FIGURE 11. System components installation space fulfilment

The front spar penetration represents a common high-lift system conflict. Conventionally used slats are generally actuated by a curved rack and pinion mechanism. To achieve the required extension distance of the slat panels, the rack necessarily penetrates the front spar and pushes into the wing tank. Structural adaptation of the spar is thus needed to enable this and the fuel tank volume is slightly compromised. Something similar is required for the outer Krueger flaps 6 and 7 examined in this study. A significant advantage arises from the fact that the outboard wing tank contains a smaller fuel volume compared to the rest of the wing. The impact on the overall fuel capacity is thus minimal.

Based on this argumentation the installation space requirement is considered fulfilled in this work. However, the resulting restrictions for other disciplines, like structural and fuel tank sizing, have to be noted. Ideally the imposed challenges resulting from the Krueger system architecture shall be reduced to a minimum. Further investigation of this topic is thus to be carried out in future work, A change of

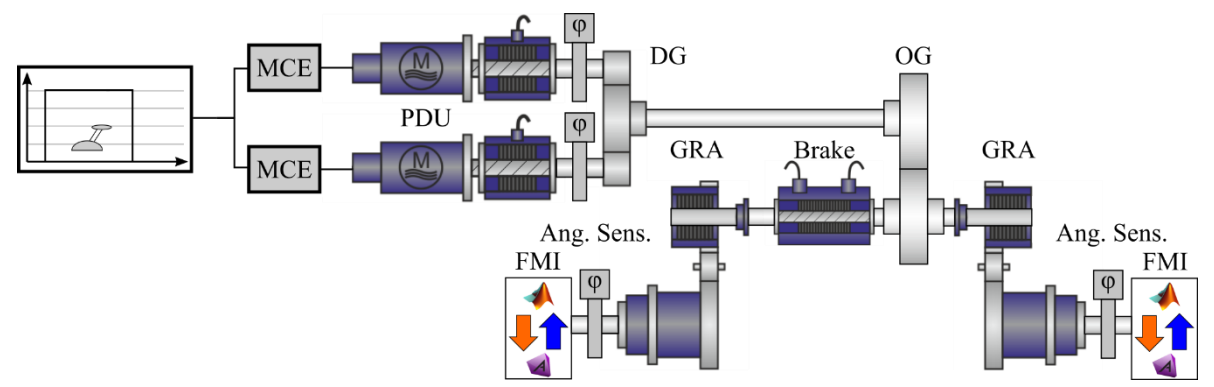


FIGURE 12. Schematic representation of the single drive system architecture model

the system architecture layout with a less conservative approach has to be considered.

5. MODELING AND SIMULATION

To evaluate the dynamic behaviour of the proposed Krueger flap system architecture and investigate the power requirements a simulation model for virtual testing has been developed. This model is divided into two sub-models. The first sub-model represents the structural components, such as the Krueger panels and the kinematic in a *MSC Adams* multi-body simulation (MBS). The second sub-model is comprised of the components of the drive system architecture. This includes the drive unit, transmission shafts, GRAs, the monitoring system, gearboxes and brakes which are modelled in *Matlab Simulink/Simscape*. These two sub-models are coupled via a functional mockup interface (FMI).

5.1. Modelling of the system architecture

An overview of the system simulation model created in *Matlab Simulink/Simscape* is depicted in figure 12. The modelling method is based on [14][15][16] but is adapted for the use for this Krueger flap high-lift system architecture. This method employs the modelling of system components as mass-spring-damper elements, incorporating aspects such as inertia, backlash and friction torque.

The virtual pilot commands a position of the leading edge devices. This signal is sent via the flight control computer (not part of this model) to the MCEs controlling and monitoring the PMSMs included in the PDU. The resulting rotational velocity of the PMSMs is controlled by a feedback-loop including the angular position sensor signals of the respective system. Additionally, the corresponding sensor signals of the neighbouring Krueger flap system architectures trigger the start of the actuation process to ensure the sequential actuation proposed in section 3. Through the speed-summing differential gear the PMSMs torque is added up, while the output speed of the gearbox is equal to the rotational velocity of the motor output shafts. The produced mechanical power is then transmitted via the transmission shaft. Two GRAs are driven by the shaft, which in turn move the kinematic and thus the Krueger panel and bullnose. Means for the detection of various failure conditions are provided by the angular position sensors. In case of failures, such as shaft disconnect or runaway, two redundant brakes inside the PDU and an additional brake on the transmission shaft decelerate and eventually stop the system in a safe state. The investigation of failure scenarios is not within the scope of this paper, therefore the brakes only increase inertia and frictional

torque on the system.

The Functional Mock-up Interface (FMI) used for cosimulation is located at the GRA outputs transferring the rotational velocity of the GRAs to the MBS of the structural elements. In turn, the simulated loads acting on the GRA resulting from aerodynamic forces and structural interactions are transferred from the MBS to the system model via the FMI.

The model for the grouped drive system for Krueger flap 3 and 4 represents the same structure, but features two additional GRAs, sensor positions, input and output parameters for transfer to the *MSC Adams* model and additional transmission shaft elements due to the actuation of two devices by one PDU.

5.2. Modelling of the structural elements

The MBS model generated in *MSC Adams* consists of the optimized goose-neck kinematics previously defined in section 3 and the Krueger flaps geometry of the reference aircraft. The model of the leading edge high-lift system is shown in figure 13. The figure also highlights the different positions of the Krueger flaps, due to the sequential actuation. In figure 13 the innermost Krueger flap 1 is already fully deployed while devices 2 to 6 are in different stages of the deployment process.

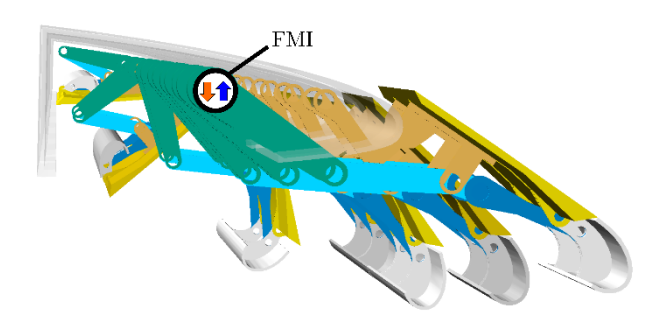


FIGURE 13. Krueger flaps model with kinematics during actuation

The Krueger flaps are divided into two parts. Panels, depicted in yellow and the bullnoses displayed in grey. As presented in section 2, the rotation of the bullnoses accelerates through the kinematic during the deployment process, which results in reduced angular movements compared to the panel in the critical transition phase leading to minimal surface area exposed to the airflow, causing minimal aerodynamic drag. This is realized by the dark blue rod depicted in figure 13, which is actuated through a lever mechanism realized through the light brown

©2024

6

hinge on the flap panel combined with the light blue rod. The GRAs of the drive system architecture are connected to the green drive lever. This represents the interfaces to the drive system model in *Matlab Simulink/Simscape* via FMI, which transfers the simulated torques acting on the respective GRAs to the drive system model and in return receiving the rotational speed of the GRAs induced by the drive system model.

All structural elements are modelled as rigid bodies and connected via standard joints. The aerodynamic loads acting on the flap panels and bullnoses, determined by the DLR, are implemented on spanwise central positions in regard to the respective body with a body-fixed load induction point via which the effective loads are applied. Each load induction point consists of normal and tangential force elements as well as a pitching moment dynamically changing depending on the Krueger flaps deflection angle. Since the current model is rigid and the actual distribution of aerodynamic forces along the span is unknown at the present time, this simplification of a single load induction point is considered acceptable.

5.3. Simulation results

An exemplary study has been conducted for the investigation of the co-simulation of the proposed drive system architecture model in *Matlab Simulink/Simscape* and the MBS model of structural elements in *MSC Adams* coupled via FMI. The considered operating case is the extension and retraction without a failure occurrence. The actuation command is shown in figure 16.

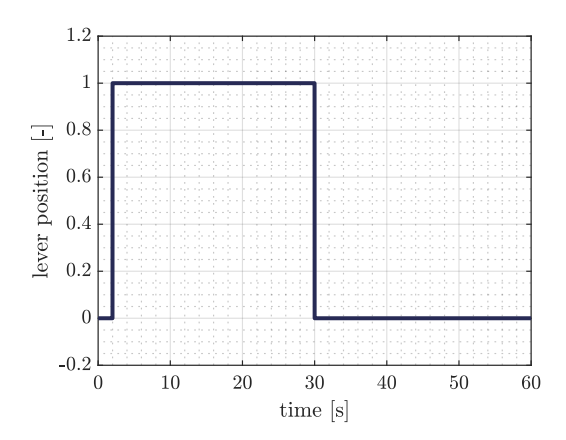


FIGURE 16. Lever position command over simulation time

As depicted in figure 16, the lever position changes from 0 to 1 at 2 seconds, which indicates the command for the deployment process of the Krueger flaps. This operation is expected to last 18.7 seconds and thus end at 20.7 seconds. At 30 seconds the lever position changes back to 0 commanding the subsequent retraction procedure of the Krueger flaps which is expected to end at 50 seconds. The static intervals between deployment and retraction as well as at the end of the simulation after the retraction process shall account for potential dynamic fluctuations of the system.

The resulting flap angle over time, shown in figure 6, indicates the sequential movement of the flaps. The resulting rotational velocity progression is depicted in figure 17. Each Krueger flap is actuated by two GRAs, which are simultaneously driven. Therefore, the depicted speeds refer to both GRAs of the respective device.

As presented in figure 17 the drive system of each

corresponding Krueger flap accelerates according to the sequential sequence reaching a maximum speed of 35 °/s. Close to reaching the deployed position the drive decelerates to a speed of 5 °/s to oppose the directory change of the aerodynamic forces, reduce the potential for instability resulting from aerodynamic fluctuations acting on the flap, safely connect the bull-nose with the panel without causing collisional damage of the structural elements and reduce required power. The ensuing retraction process follows the same principal with inverse direction of rotation. The GRA output loads were already depicted and discussed in section 4.2.

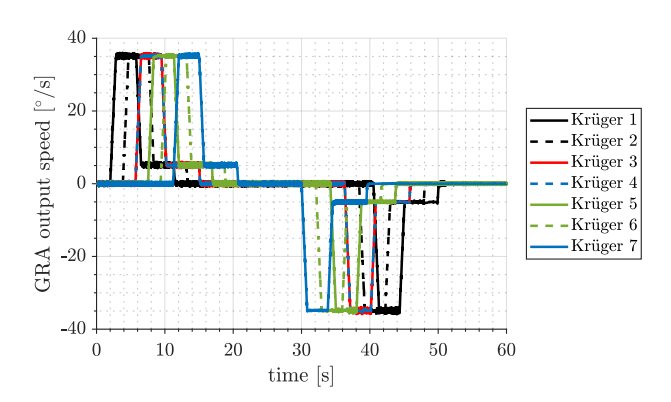


FIGURE 17. Output speed of GRAs during deployment and subsequent retraction

The resulting electrical power required by the PDUs of the respective Krueger flap drive system architectures is given in figure 18. The maximum PDU power required to drive Krueger flaps 3 & 4 of 2.6 kW is evidently the greatest compared to the other drive systems. This was to be expected due to the grouped system architecture driving two flaps instead of one and thus being exposed to greater loads acting on the transmission. The power required to drive the other Krueger flaps however decreases the further outwards the device is positioned. This has already been depicted in figure 10 showing this decrease in loads acting on the outboard positioned devices. The decrease in loads can be explained by reduced Krueger flap sizes and therefore smaller surface areas of the panels and bullnoses leading to lower aerodynamic loads.

It is noteworthy that the required power during the deployment phase differs from the retraction phase. During the deployment of the Krueger flaps, the maximum required power occurs while the device passes through the critical transition range. The peak appears at the so called 'barndoor'-position [17], where the leading edge of the Krueger flap panel is pointing downwards, perpendicular to the flow, as depicted in the middle picture shown in figure 4. The device thus produces maximum drag resulting in high loads and power requirements for the drive system architecture. The maximum negative PDU power utilized to brake the Krueger flaps close to reaching the fully deflected position is lower than the maximum positive power.

During the retraction process the aerodynamic load acting on the Krueger flaps differs compared to the deployment process as depicted in figure 10. This results in a dissimilar power progression compared to the deployment process. The maximum power occurs close to the fully deflected position and therefore at the start of each individual retraction process. The aerodynamic loads generate lift on the devices at this position, which acts in the same direction

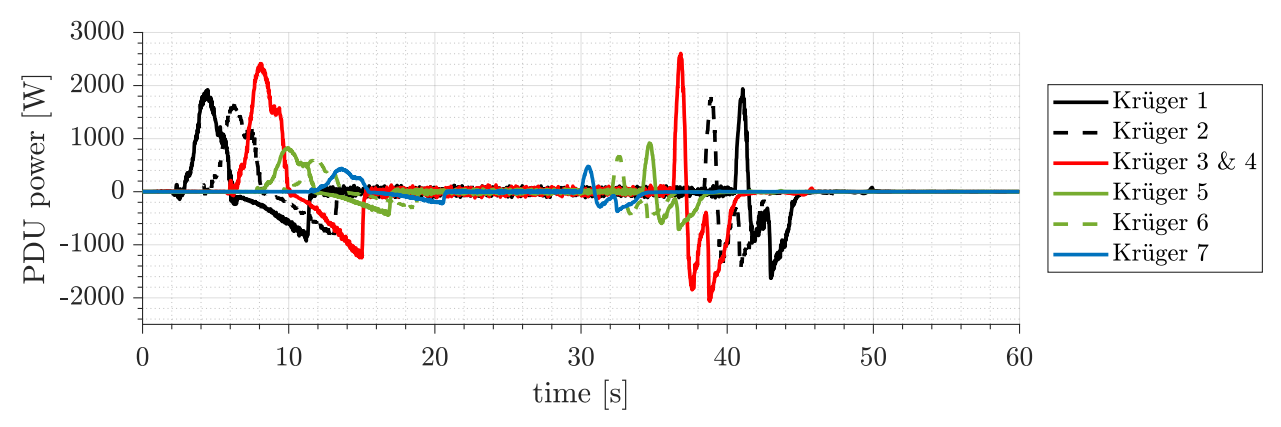


FIGURE 18. PDU power for each Krueger drive system

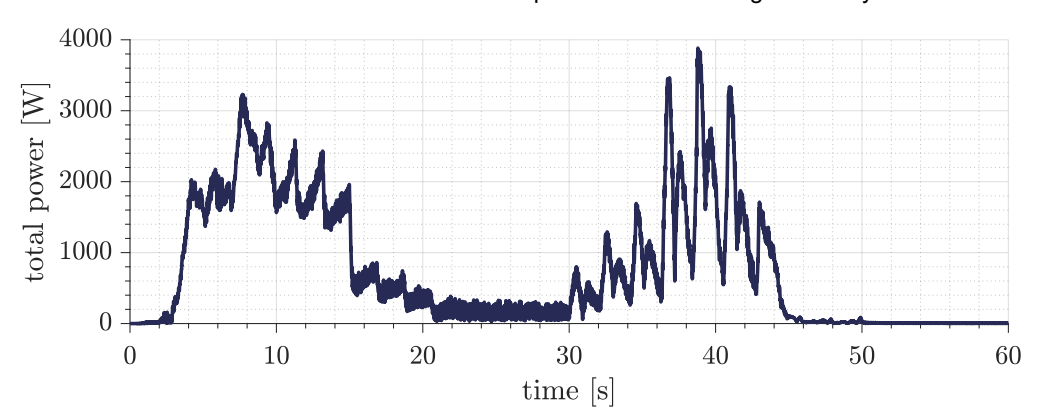


FIGURE 19. Power required for the total Krueger drive system architecture

8

of movement during deployment and thus has to be decelerated by the drive system, leading to a low negative power requirement. During retraction however, the lift acts against the direction of movement and thus has to be surpassed by the drive system to initiate the retraction process. This leads to higher required loads and a greater power demand. Additionally, the maximum negative power occurring during the retraction through the critical transition area exceeds the previously established maximum negative power occurring during deployment. Analogous to the negative power occurring during deployment, the negative power occurring during retraction is employed to brake the Krueger flaps as they approach the fully retracted position. This serves to prevent potential collisions between the devices and the wing structure.

In figure 19 the power required for the total Krueger system architecture to drive the devices on both wing sides is depicted. The absolute of the required power values was taken. Thus, it was conservatively assumed that the power used to brake the devices need to be actively supplied as positive power to the braking system. Braking via energy recovery methods, like motor recuperation, are not considered in order to depict the maximum possible power required by the total system. The absolute power data of the single systems for both wing sides were then totalised leading to the total power graph depicted in figure 19. It was observed that the total power supply during deployment results in a more continuous progression compared to the more dynamic course during retraction. This results from the deceleration of the drive system during deployment close to the maximum deflection angle. In this area the maximum aerodynamic loads act on the devices, as can be seen in figure 10. Due to the reduced rotational speed however, the required power rises only gradually, resulting

in a steadier power progression. In contrast, during retraction the Krueger flaps are driven with maximum speed in this area of highly dynamic loads, consequently leading to more irregular power requirement alternations.

Despite the differences during deployment and retraction, the total power never exceeds the 5 kW limit requirement, which was defined in section 2. The maximum power requirement for the total Krueger drive system is given by 3.9 kW. This last requirement can therefore be met as well although the investigation was conducted employing conservative assumptions. The maximum power will possibly be further reduced in future work with optimized speed limits during critical load areas. Especially at the beginning of the retraction process where high loads act opposing to the direction of movement, the actuation speed could be reduced to achieve decreased total power requirements.

6. CONCLUSION

In the present paper, a preliminary design of a drive system architecture for Krueger flaps was presented and discussed. Krueger flaps represent a critical enabler technology for future laminar wings. Even small dirt particles or insects on the wing surface can potentially create turbulence wedges preventing laminar flow. By using the proposed raised Krueger flaps as high-lift devices, the leading edge of the wing can be shielded and thus protected from particles colliding with the surface.

The reference aircraft, device segmentation and general requirements were presented. A crucial condition resulted from the critical transition range, indicating a deflection area where devices must not be jammed simultaneously. The solution of sequential actuation has been identified to

©2024

mitigate this failure condition. On the basis of the given requirements different kinematics were discussed and the drive system architecture was defined. A preliminary sizing of system architecture components was conducted to predict their mass and the required installation space as well as to investigate the overall system safety. The resulting architecture design was subsequently validated against the previously established requirements. To evaluate the dynamic behaviour of the system and review the power required to drive the devices, a co-simulation model was introduced to couple the structural dynamics of the Krueger flap and kinematics in MSC Adams with the drive system model in Matlab Simulink/Simscape. A nominal deployment and subsequent retraction process was simulated for which the results were depicted and discussed. The results indicate the technical feasibility of the proposed system.

This work focused on a preliminary analysis of an initial system architecture design for Krueger flaps to identify potential challenges, limits and future recommended actions. One of these challenges was given by the restrictive installation space. While the drive systems for the innermost Krueger flaps fit well into the wing geometry, the components of the outermost devices 6 and 7 collided with the front spar. This violation was accepted due to similar front spar interactions present at conventional leading edge devices for transport aircrafts. Nethertheless, a solution to this challenge might arise by changing the system architecture. The PDU size for example is mainly driven by the redundant motor concept. Future work is intended to focus on less conservative approaches and more optimized solutions in this regard. This includes the reduction of the number of MCE components, which produce a high maintenance effort. The established mass and power requirements were fulfilled by the proposed system architecture but shall be further optimized in future work. A more optimized drive speed progression in areas of high aerodynamic loads, while still fulfilling the required actuation time, presents one aspect to be further investigated.

ACKNOWLEDGEMENT

The results of the presented paper are part of the work in the research project Ultra high efficient wing and moveables for next generation aircraft (ULTIMATE), which is supported by the Federal Ministry of Economic Affairs and Climate Action in the national LuFo VI.2 program. Funding code for TUHH: 20A2101E. Any opinions, findings and conclusions expressed in this document are those of the authors and do not necessarily reflect the views of the other project partners.

Supported by:



on the basis of a decision by the German Bundestag

BIBLIOGRAPHY

- [1] Lynde, Michelle N., et al. "Design of a Crossflow Attenuated Natural Laminar Flow Flight Test Article." AIAA Scitech 2021 Forum. 2021.
- [2] Banchy, Michelle, Campbell, Richard, and Hiller, Brett. "Crossflow Attenuated Natural Laminar Flow (CATNLF) Technology Development: From Concept to Flight." AIAA Hampton Roads Section (HRS) Young Professionals Technical Excellence Lecture. 2022.
- [3] Seitz, Arne, A. Hübner, and Risse, Kristof. "The DLR TuLam project: design of a short and medium range transport aircraft with forward swept NLF wing." CEAS Aeronautical Journal 11.2, 2020.
- [4] Hasabnis Apurva, et al.: "The UHURA Project at a Glance Motivation and Objectives," IOP Conf. Ser.: Mater. Sci. Eng Vol. 2526:012005 (2023).
- [5] Peter K.C. Rudolph. "High-Lift Systems on Commercial Subsonic Airliners". NASA CR4746 1996.
- [6] European Aviation Safety Agency: Certification Specifications and Acceptable Means of Compliance for Large Aeroplanes: CS-25 Amendment 27, 2023.
- [7] Franke, Dirk M., and Wild, Jochen. "Aerodynamic Design of a Folded Krüger Device for a HLFC Wing." New Results in Numerical and Experimental Fluid Mechanics X: Contributions to the 19th STAB/DGLR Symposium Munich, Germany, 2014. Springer International Publishing, 2016.
- [8] Wild, Jochen, Strüber, Henning, and Vervliet, Antoon. "Krueger Design and Motion Requirements." Journal of Physics: Conference Series. Vol. 2526. No. 1. IOP Publishing, 2023.
- [9] Fox, Stephen J. and Sakurai, Seiya. "Link mechanisms for gapped rigid krueger flaps, and associated systems and methods." U.S. Patent No. 7,578,484. 2009.
- [10] S-18 Aircraft and Sys Dev and Safety Assessment Committee. Guidelines and methods for conducting the safety assessment process on civil airborne systems and equipment. SAE International. 1996.
- [11] European Aviation Safety Agency: Design Considerations for Minimizing Hazards Caused by Uncontained Turbine Engine and Auxillary Power Unit Rotor Failures AMC 20-128A. 2021.
- [12] Brombach, J., et al. "Optimized cabin power supply with a +/- 270 V DC grid on a modern aircraft." 2011 7th International Conference-Workshop Compatibility and Power Electronics (CPE). IEEE, 2011.
- [13] Rosero, J. A., et al. "Moving towards a more electric aircraft." IEEE Aerospace and Electronic Systems Magazine 22.3. 2007.
- [14] Benischke, Stefan, and Thielecke, Frank. "Evaluation of control strategies for single flap drive systems in multifunctional high lift systems". No. 2015-01-2479. SAE Technical Paper, 2015.
- [15] Neumann, Uwe. "Methoden zur signal- und modellbasierten Lastbegrenzung in verzweigten mechanischen Landeklappen-Antriebssystemen von Transportflugzeugen". Shaker, 2009.
- [16] Krall, Konstantin, et al. "Virtual testing of skew detection concepts for future leading edge slats." 9th International Conference on Recent Advances in Aerospace Actuation Systems and Components, R3ASC 2023. INSA, 2023.

[17] Ponsin, Jorge, and Lozano, Carlos. "Lattice Boltzmann Simulation of a Deploying Krueger Flap Device." Advanced Computational Methods and Design for Greener Aviation. Cham: Springer International Publishing, 2024. 111-123.